ECS Transactions, 25 (1) 15-27 (2009)
10.1149/1.3210555 ©The Electrochemical Society

Interfacial Morphology and Contact Resistance Model for Polymer Electrolyte Fuel Cells

T. Swamy[a], F. E. Hizir[a], Manish Khandelwal[a,b], E. C. Kumbur[a,c] and M. M. Mench[a,*]

[a]Fuel Cell Dynamics and Diagnostic Laboratory (FCDDL)
Department of Mechanical Engineering, The Pennsylvania State University
University Park, PA 16802 USA
[b]Current affiliation: UTC Power, South Windsor, CT 06074 USA

[c]Current affiliation: Department of Mechanical Engineering and Mechanics, Drexel University
Philadelphia, PA 19104 USA

[*]Corresponding Author (mmm124@psu.edu)

The imperfect interface between the catalyst later (CL) and micro porous layer (MPL) in a polymer electrolyte fuel cell (PEFC) results in interfacial gaps which can be considerably larger than the pores in the bulk CL and MPL. This leads to an electronic resistance and a potential pooling location for liquid water resulting in mass transport losses. In this study, an analytical model representing the CL|MPL interface under compression is developed to estimate the electrical contact resistance and to elucidate the effect of the initial surface morphology on the contact resistance and interfacial void volume. The results show that the local compression pressure, elasticity of the diffusion media and surface morphology of the mating materials are the key factors controlling the CL|MPL interfacial contact. This micro-contact model not only strengthens our understanding of the CL|MPL interface, but once integrated with a macroscopic fuel cell model, can be used to more accurately predict fuel cell performance.

Introduction

Fuel cell technology, especially polymer electrolyte fuel cells (PEFCs), is a promising alternative power source for a variety of applications. Fuel cell performance is characterized by its polarization characteristics, which comprises of electrode, ohmic and mass transport losses. A potential source for ohmic and mass transport losses originates along the various interfaces that exist between the fuel cell components, namely micro porous layer and catalyst layer (MPL|CL), MPL|DM (diffusion media) and DM|BP (bipolar plate) interfaces. In particular, the MPL|CL interface plays an important role since it shares a border with the reaction sites in the fuel cell.

Due to the inherent roughness exhibited by the MPL|CL surfaces, the contact between the two materials under compression is imperfect. This not only results in a loss in contact area, giving rise to an interfacial ohmic resistance (which can be approximately 6% of the overall ohmic resistance) [21], but also leads to the formation of interfacial gaps between the two surfaces, which could lead to mass transport losses due to liquid water pooling in the interfacial voids. Much of the fuel cell literature regarding water

management is focused on CL layer modeling [1-6] or the impact of MPL [6-13] on the capillary water transport. So far, few studies have focused on the interfacial losses in the PEFC. A few experimental studies have focused on characterizing the interfacial resistances [14-20], but the scope has been limited to losses at the BP|DM interface. Makharia *et al.* [21] attempted to evaluate the MPL|CL interfacial resistance; however the main emphasis was not placed on examining the effect of MPL|CL interfacial morphology on the contact resistance. Recently, numerical modeling has been used to estimate the interfacial losses [22, 23], but again the main focus was on the BP|DM interface. To the best of the authors' knowledge, there is no direct study that models the MPL|CL interface in particular.

Interfacial modeling has been studied extensively in the field of tribology and electrical contact mechanics [24-31]. These models are based on the Hertzian theory of contact and on probabilistic modeling techniques, to account for the stochastic nature of the mating surface profiles. The pioneer of the interfacial resistance model is R. Holm [31], who presented the theory of interaction of rough surfaces for a single contact. Later, Greenwood and Williamson [25] (GW model), extended Holm's work to span the entire mating surface area, and their work is widely used to model contact of interfaces. However, the GW model does not present a technique to evaluate all of the required input parameters for the contact model. Nayak [27] presented a statistical approach to estimate these input parameters based on surface profile information. Since these models depend on the surface profile characteristics and material properties, they can be extended to the MPL|CL interface if we can obtain reliable profile statistics.

In this work, a statistics based analytical model is presented to gain a better understanding of the MPL|CL interface. The effect of the actual MPL|CL surface morphology and mating characteristics are investigated. The model is capable of estimating the contact resistance losses at the MPL|CL interface in a PEFC under compression. A detailed parametric study is done to investigate the key parameters to minimize these losses and to quantify the void volume in the interfacial gaps. Ultimately, this model can be integrated with a macroscopic fuel cell model to more accurately predict fuel cell performance.

Method of Approach

The three key physical parameters required in the contact resistance model, which are a function of the surface profile characteristics, can be evaluated statistically if the surface profile height data are known [27]. For this purpose, we use optical profilometry (OP) as a technique to evaluate MPL|CL surface profile data, as described below.

Experimental

The surfaces of catalyst layers from membrane electrode assemblies and MPL of carbon felt type diffusion media (SGL 10BB) were separately investigated to generate surface profile characteristics. Optical profilometry was used to quantify the surface roughness and morphology of these samples. The key advantage of this imaging technique is its capability of making high-vertical-resolution, quantitative and damage-free measurements of broad areas without any contact with the surfaces. Details of the procedure are provided in [32].

Measurement results show that both MPL and CL have rough surface characteristics and possess irregularities such as high hills, large valleys and deep cracks on the surface.

However, a comparison of the roughness metrics indicates that the MPL surface is rougher in nature compared to the CL surface. It was observed that the cracks on MPL differ substantially with those in CL in terms of their orientation, size, shape, depth and density. Cracks on the CL surface are observed to be long and thin with no significant variance in the crack width, which is around 15 μm at the crack center, and aligned with respect to each other. The observed cracks have an average crack density of 3.4% ± 0.2%, and can extend through the entire CL thickness. Cracks on the MPL surface, however, are observed to be variable in width which can be as large as 60 μm, randomly oriented, and have relatively higher depth, which can be as large as the MPL thickness. Holes and dents with diameter of the order of 100 μm and variable frequency also exist on the MPL surface, which lead to a variation in the MPL areal crack density from 2.8% to 8.9% [32]. The difference between cracks or deep cuts in the CL and MPL surfaces, which some manufacturers can mostly eliminate, should be distinguished from interfacial voids, which occur as a result of surface roughness, regardless of the presence of cracks.

Model Formulation

The discrete surface data from optical profilometry measurements are converted to a continuous representation, which is fed into the model to evaluate certain key surface characteristic parameters. Finally, we obtain the MPL|CL interfacial resistance and the separation between the mean planes of the MPL and CL surfaces as output. These steps are explained in detail in the following sections.

Surface Profile Characterization

In order to obtain the interfacial morphology parameters at the MPL|CL contact, a continuous mathematical representation of the discrete surface profile data of the two surfaces is necessary. For this purpose, the Discrete Fourier Transform (DFT) algorithm was utilized to represent the discrete measured data as a sum of sine and cosine series. As an approximation, representative cross-sections of the discrete surface profile data were chosen and fed into the DFT algorithm, since 3-D surfaces require large amounts of computational time for parameter evaluation. The DFT algorithm is applied to the discrete data, $z(x)$, in the following manner:

$$Z(x) = \frac{1}{N}\sum_{n=1}^{N} C(n)\, e^{\frac{-2\pi j(n-1)(x-1)}{N}} \qquad [1]$$

where $Z(x)$ and $C(k)$ represent the continuous analytical representation, and the Fourier coefficients given by Eq. (2). N represents the number of discrete data points in each profile that is considered.

$$C(k) = \sum_{n=1}^{N} z(n)\, e^{\frac{-2\pi j(n-1)(k-1)}{N}} \qquad [2]$$

The algorithm in Eq. (1) and (2) is processed by using measured MPL and CL surface data to obtain continuous representations or MPL and CL surface profiles, $Z_{MPL}(x)$ and $Z_{CL}(x)$, respectively.

Contact Model for Smooth and Rough Surface

Figure 1 represents the contact between a smooth surface and a single summit on a rough surface. Figure 1 shows the undeflected summit and its deflected shape when a load, *P*, is applied. In order to apply the GW model to our case, we neglect the porosity of the contacting media at the MPL|CL interface, since the pore sizes are significantly less than the morphological features observed. The GW model also approximates all the MPL|CL contacts to be elastic and that the contact points are largely separated so that the interaction between them can be neglected. It is shown in literature [32] that the MPL and CL surfaces, just like any other surface, are inherently rough, with asperities distributed randomly over the entire surface.

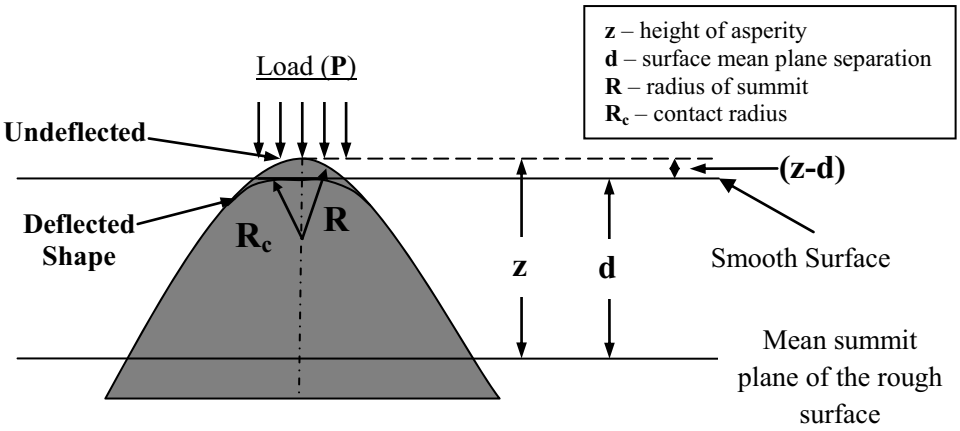

Figure 1. Contact geometry at a single summit of any rough surface with a smooth surface.

According to the Hertzian theory [24-26] of elastic contact, the load, *P*, on a single summit (Fig. 1) of height, *z,* and radius, *R,* can be evaluated as:

$$P = \frac{4}{3} E_{eq} R^{\frac{1}{2}} (z-d)^{\frac{3}{2}} \qquad z > d \qquad [3]$$

$$E_{eq} = \left[\frac{1-\upsilon_1{}^2}{E_1} + \frac{1-\upsilon_2{}^2}{E_2} \right] \qquad [4]$$

where υ_i and E_i (i = 1,2) are the Poisson's ratio and Young's modulus of the two materials in contact, respectively. Equation (4) represents the effective Young's modulus as E_{eq}. Approximating current flow across the interface to be independent due to the relatively large separation between asperities; the electrical contact conductance for a single contact can be defined as [31]:

$$g_c = \frac{4R_c}{\rho_1 + \rho_2} \qquad [5]$$

$$R_c = \sqrt{R(z-d)} \qquad [6]$$

where ρ_i (i = *1,2*) is the electrical resistivity of the materials in contact (MPL and CL) and R_c is the deformed contact radius of the summit as shown in Fig. 1.

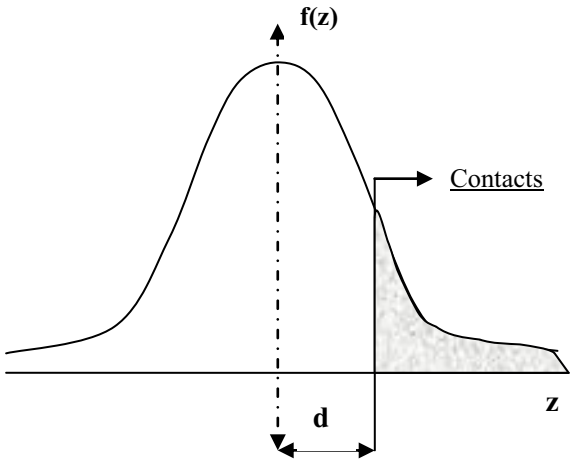

Figure 2. Gaussian distribution of summit heights.

Eq. (3) and (5) are derived for one summit, so it is necessary to extend the theory to the entire surface encompassing all the asperities. As mentioned before, three statistical parameters that describe the rough surface must be evaluated and incorporated into Eq. (3) and (5). Eq. (3) and (5) are then integrated over the whole surface. The randomly distributed asperities on the given rough surface are approximated to be spherical in shape with a constant radius, R, and have a Gaussian probability distribution as shown in Fig. 2 where σ_{sum} is the standard deviation of the summits. Let the density of summits on the surface be D_{sum}. The probability density function can be defined as [24-25]:

$$f(z) = \frac{1}{\sigma_s \sqrt{2\pi}} e^{-\frac{z^2}{2\sigma_{sum}^2}} \qquad [7]$$

Now, the probability, θ, that a randomly selected summit has a height in excess of the surface separation, d, can be expressed as:

$$\theta(z > d) = \int_d^\infty f(z)dz \qquad [8]$$

It is clear that the load, P, is a function of the random variable z. The average value of function of a random variable is obtained by integrating the product of the function in consideration and the probability density of the random variable over the domain of the random variable. Hence, averaging P over the entire surface area and evaluating the compression pressure, p, gives:

$$p = \int_d^\infty \frac{4}{3} E_{eq} D_{sum} R^{\frac{1}{2}} (z-d)^{\frac{3}{2}} f(z)dz \qquad [9]$$

Note that the average compression pressure is approximated to be uniform over the MPL|CL interface. Integrating the electrical contact conductance in Eqn. (5) over the entire contacting surface gives:

$$g = \int_{d}^{\infty} \frac{4}{\rho_1 + \rho_2} D_{sum} R^{\frac{1}{2}} (z-d)^{\frac{1}{2}} f(z) dz \qquad [10]$$

To simplify the integration in Eq. (9) and (10), the equations are written in terms of the normal probability distribution function, $\varphi(x)$

$$\varphi(x) = \frac{1}{\sqrt{2\pi}} e^{-\frac{x^2}{2}} \qquad [11]$$

The height variables are scaled for numerical convenience using σ_{sum} and after some mathematical manipulation, the following equations are obtained:

$$p = \frac{4}{3} E_{eq} D_{sum} R^{\frac{1}{2}} \sigma_{sum}^{\frac{3}{2}} F_{\frac{3}{2}}\left(\frac{d}{\sigma_s}\right) \qquad [12]$$

$$g = \frac{4}{\rho_1 + \rho_2} D_{sum} R^{\frac{1}{2}} \sigma_{sum}^{\frac{1}{2}} F_{\frac{1}{2}}\left(\frac{d}{\sigma_s}\right) \qquad [13]$$

$$r = \frac{1}{g} \qquad [14]$$

where r is the contact resistance, and

$$F_n(t) = \int_{t}^{\infty} (x-t)^n \varphi(x) dx \qquad [15]$$

where the function in Eq. (15) is evaluated by expressing it in terms of parabolic cylinder function, $U(a,t)$ [33], as:

$$F_n(t) = \frac{n!}{\sqrt{2\pi}} \frac{U(n+\frac{1}{2}, t)}{e^{\frac{t^2}{4}}} \qquad [16]$$

It is clear from Eq. (12), (13) and (14) that the compression pressure and the contact resistance are a function of the material properties incorporated in E_{eq}, and the three main statistical properties of the mating surfaces (D_{sum}, R and σ_{sum}). Since the material properties are known, evaluation of these main statistical parameters is necessary to predict the interfacial resistance of the mating surfaces.

The material properties of the MPL and CL are reported in Table I. Since this is a layered contact problem, and the materials (MPL and CL) forming the interface are very thin, the Young's modulus is approximated with that of the DM, since it is the DM that plays the role of a backing material for the interface in consideration. This implies that

the MPL and CL layers conform to the deformation in the DM due to the applied compression pressure.

TABLE I. Material properties for the backing and interface materials

Properties	Material	Value	Units
Young's Modulus[34]	DM	10,000	MPa
Electrical conductivity[35] (through plane)	MPL	300	$S.m^{-1}$
Electrical conductivity[35] (through plane)	CL	200	$S.m^{-1}$

In order to evaluate the parameters R, σ_{sum} and D_{sum}, the following statistical manipulation is performed [27]. Consider $Z(x)$, the analytical function derived in Eq. (1), which represents a continuous surface profile. At this juncture, the surface is approximated to be isotropic. The auto-correlation function (ACF), $A(x)$, is defined as [27]:

$$A(x) = \lim_{L\to\infty}\left[\frac{1}{2L}\left(\int_0^L Z(x)Z(x+j)dj\right)\right] \quad [17]$$

where L is the length of the profile. The power spectral density function (PSDF), $\Phi(k)$, can be defined as the Fourier transform of the ACF as [27]:

$$\phi(k) = \frac{1}{2\pi}\left[\int_{-\infty}^{\infty} A(x)e^{-\frac{2\pi ikx}{N}}dx\right] \quad [18]$$

where k is the wave number of the spectral component that constitutes the surface profile. The Spectral moments, m_0, m_2 and m_4, of the PSDF are defined as [27]:

$$m_i = \int_{-\infty}^{\infty} k^i \phi(k)dk \quad (i = 0,2,4) \quad [19]$$

The bandwidth parameter, α, which depends on the shape and the extent of the spectrum of the roughness profile, is defined as [27]:

$$\alpha = \frac{m_0 m_4}{(m_2)^2} \quad [20]$$

It was shown [27] that the parameters R, σ_{sum} and D_{sum} can be expressed solely as a function of the spectral moments (m_0, m_2 and m_4) and the bandwidth parameter α. The corresponding relations are shown below:

$$R = \frac{3}{8}\left(\frac{\pi}{m_4}\right)^{\frac{1}{2}} \quad [21]$$

$$\sigma_{sum} = \left[\left(1 - \frac{0.8968}{\alpha}\right)m_0\right]^{\frac{1}{2}} \quad [22]$$

$$D_{sum} = \frac{1}{6\pi\sqrt{3}}\left(\frac{m_4}{m_2}\right) \quad [23]$$

Contact Model for Two Rough Surfaces

It has been shown [28, 29] that the contact of two rough surfaces is negligibly different from the contact of a smooth and an equivalent rough surface. Hence, given the values of m_0, m_2 and m_4 of the two rough surfaces in consideration *i.e.* the MPL and CL surfaces, the corresponding values for the equivalent rough surface can be computed in terms of their respective sums, *i.e.*

$$(m_0)_{eq} = (m_0)_{MPL} + (m_0)_{CL} \quad [24]$$

$$(m_2)_{eq} = (m_2)_{MPL} + (m_2)_{CL} \quad [25]$$

$$(m_4)_{eq} = (m_4)_{MPL} + (m_4)_{CL} \quad [26]$$

Where the equivalent bandwidth parameter, $(\alpha)_{eq}$, can be written as:

$$(\alpha)_{eq} = \frac{(m_0)_{eq}(m_4)_{eq}}{(m_2)_{eq}^{\ 2}} \quad [27]$$

The equivalent values of m_0, m_2, m_4 and α, are evaluated and substituted into Eq. (21), (22) and (23) to obtain the statistical parameters R, σ_{sum} and D_{sum}. Using the equivalent surface parameters shown above, we can solve for the rough-rough surface contact problem at hand by using the equations for a smooth-rough surface contact derived in the previous sections. Since the compression pressure applied to the fuel cell is known, the surface separation, d, can be evaluated from Eq. (12). Knowing the surface separation, d, the conductance, g, and the MPL|CL interfacial resistance, r, can be evaluated from Eq. (13) and (14).

Results and Discussion

The analytical model described in the previous section is used to establish the dependence of the MPL|CL interfacial resistance on the profile characteristics, the material properties of the mating surfaces and the compression pressure applied on the fuel cell. Figure 3 shows the predicted MPL|CL interface under homogeneous compression of 1.5 MPa, using actual measured cross-sections of the MPL and CL surfaces. The deep cracks in the MPL and CL are clearly visible, and it was observed that some of the cracks in the CL penetrate the entire layer. Neglecting extremely deep cracks, the average peak-to-peak surface height for MPL and CL are 25 μm and 10 μm respectively. The separation between mean planes was found to lie in the range of 5-10 μm. The maximum gap width was found to be close to 20 μm. It is evident from Fig. 3 that the MPL|CL interfacial gaps are relatively larger in dimension compared to the average pore size in the two layers. This observation suggests that the MPL|CL interface has potential to store liquid water in its gaps, which could result in significant mass transport losses across the interface. Further investigations for quantifying the mass transport losses at the MPL|CL interface is a part of the future work of this study.

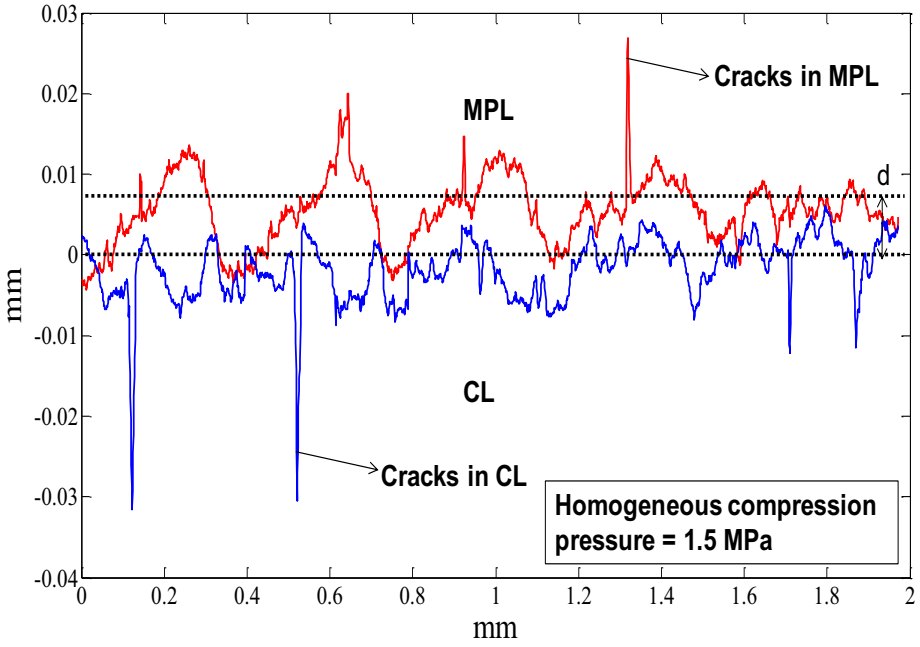

Figure 3. A typical MPL|CL interface cross-section.

Figure 4(a) shows the variation of the predicted MPL|CL contact electronic resistance as a function of the applied compression pressure. The variation in the result due to different degrees of roughness of the mating surface profiles is also simulated and shown in Fig. 4(a). For a single MPL|CL interface, under normal operating conditions of 1.5 MPa (which exists under the land), the model predicts the MPL|CL contact resistance to be around 1.8 $m\Omega.cm^2$. This result is in good agreement with the experimental result obtained by Makharia *et. al.* [21], as the error between the reported experimental value and the model prediction is around 5%. It can be seen from Fig. 4(a) that lowering the roughness of the MPL and CL surfaces by 50% results in a 40% drop in the MPL|CL interfacial resistance. This high drop in the contact resistance can be attributed to the fact

that as the roughness of the mating surfaces is decreased, or in other words, the surfaces are made relatively smoother, the number of contact points is increased, thereby facilitating electron flow across the MPL|CL interface. It should also be noted that, since the MPL surface exhibits a higher degree of roughness [32] when compared to the CL, the surface characteristics of the MPL layer dominate the surface structure at the interface, and consequently the MPL|CL contact resistance.

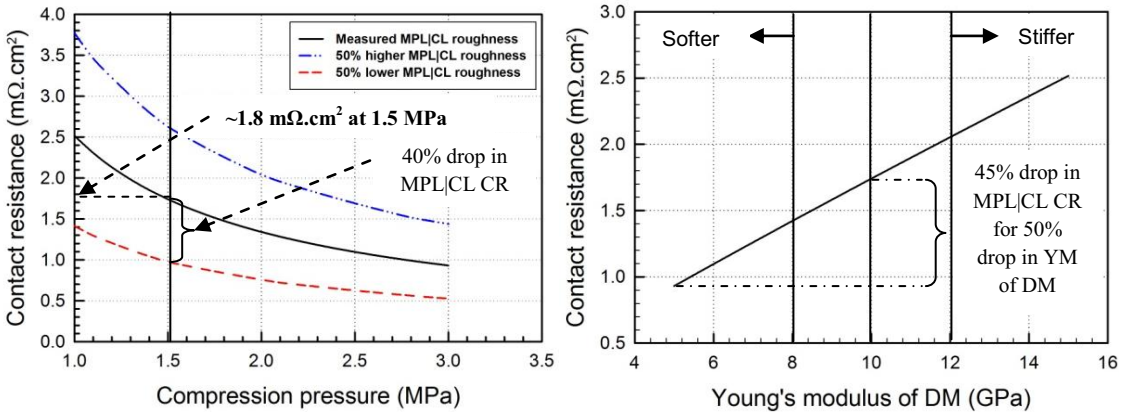

(a) (b)

Figure 4. (a) Predicted MPL|CL contact resistance (CR) vs compression pressure (CP) at different degrees of surface roughness, (b) Predicted MPL|CL contact resistance vs Young's modulus (YM) of DM.

Figure 4(b) shows that the impact of the variation of the Young's modulus of the backing DM on the MPL|CL contact resistance for a homogeneous compression pressure of 1.5 MPa. It can be seen from Fig. 4(b) that the Young's Modulus has a significant effect on the MPL|CL interfacial resistance since the model predicts a 45% drop in the contact resistance with a 50% drop in the Young's modulus of the DM. This strong dependence of the contact resistance on the material property of the backing layer can be attributed to the fact that a drop in the Young's modulus of the DM results in the softening of the material, which allows the thin MPL and CL surfaces to exhibit a higher degree of conformation. This provides flexibility to the MPL and CL surfaces which locally enhances the mating percentage resulting in higher contact points, leading to a relatively lower MPL|CL contact resistance.

Figure 5 shows the variation of predicted MPL|CL contact resistance under one set of land and channel configuration. The non-homogeneous compression pressure data were predicted by combining the DM thickness-compression pressure data and the stress strain curve of the DM, given in [16, 18, 20]. Since the DM thickness measurement was performed *ex-situ* for one set of land and channel, Fig. 5 shows a continuous increase in the MPL|CL contact resistance under the channel. If the right hand boundary is another landing instead of a continued channel, the contact resistance is expected to peak half way into the channel, as shown in Fig. 6. The model predicts that there is approximately 1000% increase in the MPL|CL contact resistance at mid-channel as compared to contact resistance under the land. This drastic increase can be attributed to the fact that as we move into the channel and away from the land, the compression pressure drops quite drastically and is minimal at mid-channel. The model also predicts a high value of MPL|CL contact resistance locally at the land|channel interface, which can be attributed

to the fact that there is a discontinuous transition from the land to the channel due to the straight edges of the land. This results in a local drop in the compression pressure at the land|channel interface into the channel, resulting in a high local MPL|CL contact resistance. This effect could be negated by rounding the edges of the land to provide a continuous transition at the land|channel interface.

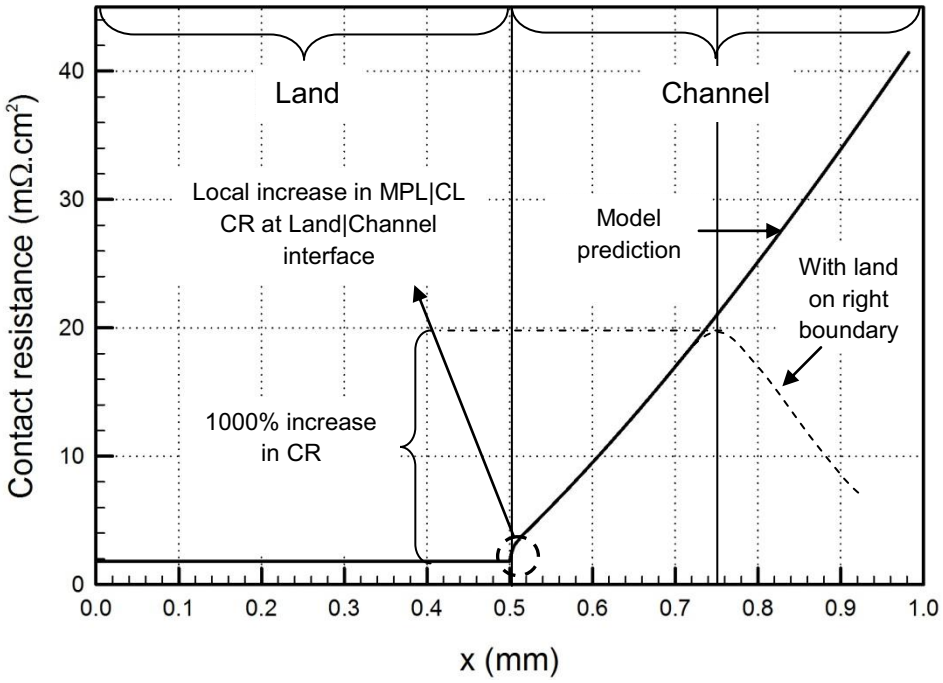

Figure 5. Predicted MPL|CL contact resistance vs distance (x) under land and channel

Summary and Conclusions

An analytical model was developed to investigate the effect of surface morphology of the mating surfaces and the applied compression pressure on the electronic contact resistance at the MPL|CL interface. Results show that the roughness of the mating surfaces and the elastic modulus of the backing DM layer have a significant impact on the MPL|CL contact resistance. The model predicts that a 50% drop in the MPL and CL surface roughness results in a 40% drop in the MPL|CL contact resistance. Since the MPL surface exhibits a higher degree of roughness when compared to the CL, the surface characteristics of the MPL layer dominate the surface structure at the interface and the MPL|CL contact resistance. Also, a 50% drop in the Young's Modulus of DM was predicted to result in a 45% drop in the MPL|CL interfacial resistance. Due to the variation in the compression pressure under the land and the channel, the MPL|CL contact resistance is predicted to be nearly 1000% higher in the middle of the channel compared to under the land. The model also predicts a high value of MPL|CL contact resistance locally at the land|channel interface, which can be attributed to a discontinuous transition from the land to the channel due to the straight edges of the land, resulting in a local drop in the compression pressure, and consequently, higher MPL|CL contact resistance. This effect could be negated by rounding the edges of the land to provide a continuous transition at the land|channel interface. Further studies are aimed at quantifying the void volume in the interfacial gaps and investigating the effect of surface

roughness and other key characteristics of the mating surfaces on the mass transport losses at the MPL|CL interface.

Acknowledgements

This study was supported by the Toyota Motor Corporation, Japan. T. Swamy would like to thank Dr. Liming Chang, Professor of Mechanical Engineering at The Pennsylvania State University, for providing useful insight in developing the contact model.

Nomenclature

Symbol	Parameter	Unit
MPL	Micro-porous layer	-
CL	Catalyst layer	-
DM	Diffusion media	-
DFT	Discrete Fourier Transform	-
GW	Greenwood and Williamson	-
z	Height of asperity	mm
Z	Analytical representation of the surface profile data	-
j	Complex number, ($\sqrt{-1}$)	Unitless
p	Compression pressure	MPa
P	Compression load	kg
d	Surface mean plane separation	mm
θ	Probability	Unitless
R	Radius	mm
E_i	Young's Modulus, (i = 1, 2)	MPa
ν_i	Poisson's ratio, (i = 1, 2)	Unitless
ρ_i	Resistivity, (i = 1, 2)	Ω.mm
σ	Standard deviation	mm
D	Density of summits on the surface	mm^{-2}
g	Conductance	$m\Omega^{-1}.cm^{-2}$
r	Resistance	$m\Omega.cm^2$
λ	Roughness	μm
f	Gaussian distribution	Unitless
φ	Normal distribution	Unitless
m	Spectral moment, (i = 0,2,4)	$mm^{(i-2)}$
α	Bandwidth parameter	Unitless
eq	Equivalent	-
c	Contact (single)	-
sum	Summit	-
a	Average	-
q	Root mean square	-
t	Maximum height of the surface	-

References

1. V. Gurau, T. A. Zawodzinski, J. A. Mann, *J. Fuel Cell Sci. Technol.,* **5** (2), 021009 (2008).
2. L. You, H. Liu, *Int. J. Heat Mass Transfer,* **45** (11), 2277 (2002).
3. C. Marr, X. Li, *J. Power Sources,* **77** (1), 17 (1999).
4. D. M. Bernardi, M. W. Verbrugge, *AIChE J.,* **37** (8), 1151 (1991).

5. T. E. Springer, M. S. Wilson, S. Gottesfeld, *J. Electrochem. Soc.,* **140** (12), 3513 (1993).
6. M. M. Mench, *Fuel Cell Engines*, John Wiley & Sons (2008).
7. J. H. Nam and M. Kaviany, *Int. J. Heat Mass Transfer,* **46** (24), 4595 (2003).
8. U. Pasaogullari and C. Y. Wang, *Electrochim. Acta,* **49** (25), 4359 (2004).
9. A. Z. Weber and J. Newman*, J. Electrochem. Soc.,* **152** (4), A677 (2005).
10. Z. Qi and A. Kaufman, *J. Power Sources,* **109** (1), 38 (2002).
11. G. Lin and T. V. Nguyen, *J. Electrochem. Soc.,* **153** (2), A372 (2006).
12. U. Pasaogullari, C. Y. Wang and K. S. Chen, *J. Electrochem. Soc.,* **152** (8), A1574 (2005).
13. G. J. M. Janssen and M. L. J. Overvelde, *J. Power Sources,* **101** (1), 117 (2001).
14. B. Avasarala, P. Haldar, *J. Power Sources*, **188** (1), 225 (2009).
15. I. Nitta, O. Himanen, M. Mikkola, *Electrochem. Commun.*, **10** (1), 47 (2008).
16. I. Nitta, S. Karvonen, O. Himanen, M. Mikkola, *Fuel Cells 00*, 0000, No. 0, 410 (2008).
17. I. Nitta, T. Hottinen, O. Himanen, M. Mikkola, *J. Power Sources,* **171**, 26 (2007).
18. T. Hottinen, O. Himanen, S. Karvonen, I. Nitta, *J. Power Sources,* **171**, 113 (2007).
19. J. Kleemann, F. Finsterwalder, W. Tillmetz, *J. Power Sources,* 190, 92 (2009).
20. V. Mishra, F. Yang, R. Pitchumani, *ASME J. Fuel Cell Sci. Technol.*, **1**, 2 (2004).
21. R. Makharia, M. F. Mathias and D. R. Baker*, J. Electrochem. Soc*., **152** (5), A970 (2005).
22. Y. Zhou, G. Lin, A. J. Shih, S. J. Hu, *J. Power Sources*, **163**, 777 (2007).
23. X. Lai, D. Liu, L. Peng, J. Ni, *J. Power Sources,* **182**, 153 (2008).
24. J. I. McCool, *Wear*, **107** (1), 37(1986).
25. J. A. Greenwood and J. W. P Williamson, *Proc. R. Soc. London*, Ser. A, **295**, 300 (1966).
26. J. A. Greenwood, *Wear*, **262** (1-2), 225 (2007).
27. P. R. Nayak, *J. Lubr. Tech.*, **93**, 398 (1971).
28. A. W. Bush, R. D. Gibson and T. R. Thomas, *Wear*, **35** (1), 87 (1975).
29. M. O'Callaghan and M. A. Cameron, *Wear*, **36**, 79 (1976).
30. L. Chang, *J. Engineering Tribology, Proc. IMechE* Vol. **223** Part J, in press.
31. R. Holm, *Electrical Contacts Handbook*, Springer-Verlag (1958).
32. F. E. Hizir, T. Swamy, S. O. Ural, E. C. Kumbur, M. M. Mench, *Proceedings of the 7th International Conference on Fuel Cell Science Engineering and Technology*, 85092 (2009), in press.
33. M. Abramowitz, I. A. Stegun, *Handbook of Mathematical Functions*, Vol. 55, Applied Mathematics Series, U.S. Department of Commerce, Springfield, VA (1964).
34. A. Kusoglu, A. M. Karlsson, M. H. Santare, S. Cleghorn, W. B. Johnson, *J. Power Sources,* **161**(2), 987 (2006).
35. S. Kim, M. Khandelwal, C. Chacko and M. M. Mench, *J. Electrochem. Soc.*, **156** (1), B99 (2008).